AN ENERGY CONSERVING FINITE DIFFERENCE SCHEME FOR THE SIMULATION OF COLLISIONS IN SNARE DRUMS

Alberto Torin[*]
Acoustics and Audio Group
University of Edinburgh
Edinburgh, UK
A.Torin@sms.ed.ac.uk

Brian Hamilton
Acoustics and Audio Group
University of Edinburgh
Edinburgh, UK
brian.hamilton@ed.ac.uk

Stefan Bilbao
Acoustics and Audio Group
University of Edinburgh
Edinburgh, UK
sbilbao@staffmail.ed.ac.uk

ABSTRACT

In this paper, a physics-based model for a snare drum will be discussed, along with its finite difference simulation. The interactions between a mallet and the membrane and between the snares and the membrane will be described as perfectly elastic collisions. A novel numerical scheme for the implementation of collisions will be presented, which allows a complete energy analysis for the whole system. Viscothermal losses will be added to the equation for the 3D wave propagation. Results from simulations and sound examples will be presented.

1. INTRODUCTION

Physics-based simulation of musical instruments is now an active research topic, both for acoustical studies and sound synthesis, and various numerical techniques can now tackle a wide range of complex systems. Percussion instruments, and drums in particular, with their various interacting components, constitute attractive and challenging target problems. From the first attempts at simulating single membranes in 2D, research has rapidly moved towards the simulation of complete instruments (see [1] for a review.) In recent years, a physical model for nonlinear circular membranes with snares has been proposed [2]. Finite difference methods have been employed to model timpani drums [3], snare drums [4] and nonlinear double-headed drums (i.e., tom toms and bass drums) [5].

In this paper, a physics-based simulation of a snare drum will be presented. The model consists of two membranes (batter and carry head), coupled with the surrounding air and connected by a rigid shell. A set of snares (thin metal wires) is placed below the carry head, in contact with it. In the present work, a novel energy conserving scheme for the simulation of collisions between the snares and the resonant membrane will be presented. This constitutes a major improvement with respect to previous attempts [4], for which numerical stability is not guaranteed (and is indeed a problem in implementation.) A similar approach can be adopted for the mallet-membrane interaction, which is included in this model, thus giving an energy conserving scheme for the whole system. When used as a sound synthesis tool, the usual 3D scheme describing the acoustic field produces artefacts that harm the quality of the sound. This problem can be addressed by adopting a more realistic model of 3D wave propagation that includes viscothermal losses.

A major issue broached in this paper is the numerical simulation of collisions, which play an important role in many fields, including engineering and computer graphics, and the literature on the subject is abundant (see [6] for a review). A mainstream approach for collision detection in many applications is the use of penalty-based methods, based on repulsive forces generated by slight interpenetration between the objects. In musical acoustics, many instruments rely on collisions for the production of sound, with an obvious example given by percussions. Several approaches have been used in the past, and in many cases this type of interaction has been modelled as a nonlinear Hertzian force depending on the mutual penetration of the colliding objects [7]. This model has been successfully adopted, e.g., for the simulation of the hammer-string interaction in pianos [8, 9].

For totally elastic collisions, these methods could be considered as unphysical, as they allow interpenetration in otherwise rigid bodies, and simulations of collision without the need for contact forces have been proposed [10]. Nonetheless, penalty-based methods have many advantages, as they offer a mathematically tractable and phenomenologically accurate description of the behaviour of the system, and will therefore be adopted in this study. Furthermore, the maximum penetration allowed can be bounded by choosing suitable values for the coefficients. When it comes to numerical schemes, the risk of instability is always present, and is particularly pronounced for rigid collisions. Energy-based finite difference approaches, which have a long history [11, 12], provide useful analysis tools in this sense but, for nonlinear interactions, existence and uniqueness of a solution are not always guaranteed. For the particular choice of penalty force used in this work, however, a uniqueness result has been proved recently in the case of a mass in contact with a rigid barrier [13].

This paper is organised as follows: a brief description of the

[*] This work was supported by the European Research Council, under grant StG-2011-279068-NESS.

underlying physical model will be given in Sec. 2, while its numerical implementation using finite difference methods will be discussed in Sec. 3. Sec. 4 presents an analysis of the implementation of the collision scheme; finally, some results and sound examples will be shown in Sec. 5.

2. DESCRIPTION OF THE MODEL

The geometry of the snare drum model under consideration is shown in Figure 1. Two circular membranes of equal radius R are positioned within a finite enclosure $\mathcal{V}$ of air, with which they are coupled. They are placed parallel to one another with centres along the z axis, and are defined over regions $\mathcal{M}_b$ at $z = z_b$ and $\mathcal{M}_c$ at $z = z_c$, respectively, with

$$\mathcal{M}_b = \mathcal{M}_c = \left\{(x, y) \,|\, x^2 + y^2 \leq R^2\right\}. \tag{1}$$

A rigid cylindrical cavity connects the membranes, by enclosing the portion of air between them ($z_c \leq z \leq z_b$).

As mentioned before, the important feature of snare drums is the presence of a set of snares in contact with the resonant membrane. Generally, these are 12-15 in number. For the sake of simplicity and to avoid the proliferation of notation, the following analysis will concentrate on a single snare of length L defined over a 1D domain $\mathcal{D}_s$. In implementation, however, it is straightforward to include several snares in the model.

The upper membrane is struck by a mallet, modelled as a lumped object, while the bottom membrane, together with the snare, is set into motion by the air pressure inside the cavity generated by the blow. Absorbing conditions are applied at the walls of the air box $\mathcal{V}$.

As a similar model has been employed already [4], some of the details of the system will be omitted here.

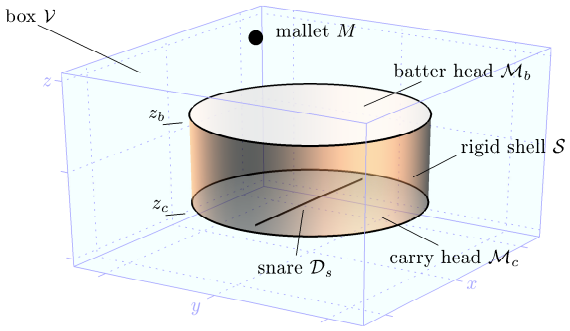

Figure 1: *Geometry of the model.*

2.1. Membranes

Let the index $i = b, c$ identify batter and carry head, respectively. The transverse displacements $w_i = w_i(x, y, t)$ of the membranes at some position $(x, y) \in \mathcal{M}_i$ and time t can be described by lossy wave equations with additional terms due to coupling conditions with the air and external collision forces. Batter and carry membrane equations read, respectively:

$$\rho_b \partial_{tt} w_b = \mathcal{L}_b[w_b] + \mathcal{F}_b^+ + \mathcal{F}_b^- + \mathcal{F}_M, \tag{2}$$

$$\rho_c \partial_{tt} w_c = \mathcal{L}_c[w_c] + \mathcal{F}_c^+ + \mathcal{F}_c^- + \mathcal{F}_s + \mathcal{F}_0 + \mathcal{F}_L. \tag{3}$$

with

$$\mathcal{L}_i[w_i] = T_i \Delta_{2D} w_i - 2\rho_i \sigma_{0,i} \partial_t w_i + 2\rho_i \sigma_{1,i} \Delta_{2D} \partial_t w_i, \tag{4}$$

where $\Delta_{2D} = \partial_{xx} + \partial_{yy}$ is the 2D Laplacian operator in Cartesian coordinates and ∂_t denotes partial time differentiation. $\mathcal{L}_i[w_i]$ groups together the linear terms in the wave equation, while the other terms are the air pressure exerted above ($\mathcal{F}_i^+$) and below ($\mathcal{F}_i^-$) each membrane. The last term $\mathcal{F}_M$ in (2) describes the mallet-membrane interaction. The equation for w_c is almost identical to (2), except for the form of the collision term $\mathcal{F}_s$ and for the presence of two additional terms $\mathcal{F}_0$ and $\mathcal{F}_L$ resolved at the two ends of the string attached to the membrane (see Sec. 2.5). The explicit expression for the coupling and collision terms will be discussed below, while the various physical parameters in (2), (3) and (4) are listed in Table 1. Additional terms, like stiffness or tension modulation nonlinearities, could be easily included in this model. For the sake of simplicity, their discussion is omitted in this work.

At the rim of both membranes, fixed boundary conditions are applied.

Table 1: *List of physical parameters used in this model.*

Membranes ($i = b, c$)	
$w_i(x, y, t)$	membrane displacement (m)
T_i	tension (N/m)
ρ_i	surface density (kg/m^2)
$\sigma_{0,i}$	frequency independent loss coefficient (1/s)
$\sigma_{1,i}$	frequency dependent loss coefficient (m^2/s)
Air	
$\Psi(x, y, z, t)$	acoustic velocity potential (m^2)
c_a	wave speed (m/s)
ρ_a	density (kg/m^3)
σ_a	viscothermal loss coefficient (m)
Mallet	
$z_M(t)$	mallet position (m)
M	mass (kg)
κ_M	stiffness parameter (N/m$^\alpha$)
α	nonlinear exponent
Snare	
$u(\chi, t)$	snare displacement (m)
T_s	tension (N)
ρ_s	linear density (kg/m)
$\sigma_{0,s}$	frequency independent loss coefficient (1/s)
$\sigma_{1,s}$	viscosity coefficient (m^2/s)
κ_s	stiffness parameter (N/m$^\beta$)
β	nonlinear exponent

2.2. Air

In this model, the equation for air propagation adopted is:

$$\partial_{tt} \Psi = c_a^2 \Delta_{3D} \Psi + c_a \sigma_a \Delta_{3D} \partial_t \Psi, \tag{5}$$

where $\Psi(x, y, z, t)$ is an acoustic velocity potential as in [14] and $\Delta_{3D} = \partial_{xx} + \partial_{yy} + \partial_{zz}$ is the 3D Laplacian operator. The coefficient σ_a for viscothermal losses generally depends on various physical parameters, among which temperature and humidity, but values for it generally lie in the range of 10^{-7} to 10^{-6} m [14].

The drum shell $\mathcal{S}$ is modelled as a rigid, reflective boundary encircling the cylindrical region between the membranes. This can be obtained by imposing the normal derivative of Ψ to be zero across the shell:

$$\mathbf{n} \cdot \nabla_{3D} \Psi = 0. \tag{6}$$

where ∇_{3D} is the gradient and $\mathbf{n}$ is the unit vector normal to the shell surface. Absorbing conditions are applied over the boundaries $\partial\mathcal{V}$ of the computational region. In this work, first order Engquist-Majda conditions will be adopted [15], as they are easy to implement within an energy-based framework. Another possibility is the use of PMLs [16].

2.3. Coupling conditions

Coupling conditions between the membranes and air can be obtained by imposing the continuity of pressure and velocity at the interface. In terms of Ψ, these conditions may be written as:

$$\mathcal{F}_i^+ = -\rho_a \lim_{z \to z_i^+} \partial_t \Psi \mid_{\mathcal{M}_i} \qquad \mathcal{F}_i^- = \rho_a \lim_{z \to z_i^-} \partial_t \Psi \mid_{\mathcal{M}_i}, \tag{7}$$

$$\partial_t w_i = - \lim_{z \to z_i^-} \partial_z \Psi \mid_{\mathcal{M}_i} = - \lim_{z \to z_i^+} \partial_z \Psi \mid_{\mathcal{M}_i} . \tag{8}$$

These conditions hold over the membrane regions $\mathcal{M}_b$ and $\mathcal{M}_c$.

2.4. Mallet interaction

The mallet exciting the membrane is modelled as a lumped, but not necessarily point-like object, with mass M and position $z_M(t) \in \mathbb{R}$ measured relatively to z_b. Let the contact region over $\mathcal{M}_b$ be defined by a distribution $g_b(x, y)$, with $\int_{\mathcal{M}_b} g_b = 1$. For a mallet striking the membrane from above, the equation of motion and the collision term appearing in (2) can be written as:

$$M \ddot{z}_M = f_M, \qquad \mathcal{F}_M = -g_b \, f_M, \tag{9}$$

where the dot symbol represents total time differentiation. It is usual in the literature to express the collision force f_M as a power law in terms of the mutual interpenetration η of the two objects [3, 7]:

$$f_M = \kappa_M [\eta]_+^\alpha, \quad \eta = \int_{\mathcal{M}_b} g_b \, w_b dx \, dy - z_M \tag{10}$$

with stiffness parameter $\kappa_M > 0$ and $\alpha > 1$, and which is active only when $\eta > 0$; the symbol $[\,\cdot\,]_+$ is used in this article to indicate the positive part, $[\eta]_+ = (\eta + |\eta|)/2$. Such an approach traces its origins in the work of Hertz at the end of 19th century (see [6] for a historical review.)

An equivalent approach, which leads to an energy conserving numerical scheme (see below), is to express the collision force f_M as the derivative of a potential Φ_M, which again will depend on the average distance η between the mallet and the membrane:

$$f_M = \frac{d\Phi_M}{d\eta} = \frac{\dot{\Phi}_M}{\dot{\eta}}, \qquad \Phi_M = \frac{\kappa_M}{\alpha + 1} [\eta]_+^{\alpha+1}. \tag{11}$$

2.5. Snare

A single snare can be modelled as a 1D string with internal losses and an additional term describing the collisions with the membrane. The equation of motion can thus be written as:

$$\rho_s \partial_{tt} u = T_s \partial_{\chi\chi} u - 2\sigma_{0,s} \partial_t u + 2\sigma_{1,s} \partial_{\chi\chi} \partial_t u - \mathcal{F}_e. \tag{12}$$

Note the change of sign in the collision force density $\mathcal{F}_e$, as in this case the string is striking the membrane from below. A stiffness term could be included as well, without complicating too much the implementation. As before, in order to define a function $G_s(x, y)$ that distributes collisions over the membrane, it is necessary to introduce a two-element affine mapping $\boldsymbol{\pi}(\chi) : \mathcal{D}_s \to \mathcal{M}_s$, from the 1D domain of the snare to the resonant membrane, that projects each point of the string onto the corresponding point on the membrane above it. A natural choice for G_s is

$$G_s(\mathbf{x}, \chi) = \delta^{(2)}(\mathbf{x} - \boldsymbol{\pi}(\chi)), \tag{13}$$

where $\mathbf{x} = (x, y)$ and $\delta^{(2)}$ is a 2D Dirac delta function. The collision density $\mathcal{F}_s$ can thus be written as

$$\mathcal{F}_s = \int_{\mathcal{D}_s} G_s(\mathbf{x}, \chi) \mathcal{F}_e(\chi) d\chi. \tag{14}$$

Analogously to the mallet-membrane case, $\mathcal{F}_e(\chi)$ can be written in terms of a distributed potential $\Phi_s(\chi)$:

$$\mathcal{F}_e(\chi) = \frac{\partial_t \Phi_s}{\partial_t \xi}, \tag{15}$$

with

$$\Phi_s(\chi) = \frac{\kappa_s}{\beta + 1} [\xi]_+^{\beta+1}, \qquad \xi(\chi) = u - \int_{\mathcal{M}_c} G_s \, w_c \, dx \, dy. \tag{16}$$

Once again, note the change in sign in the definition of $\xi(\chi)$ compared to the corresponding quantity η.

The choice of perfectly elastic collisions between the snare and the membrane must be considered only as a starting point for simulation. More refined models that introduce damping in contact forces can be adopted, like that proposed by Hunt and Crossley [17], and could be perceptually important in determining the decay time of the sound. This model requires, however, an experimental investigation of the loss coefficient, which is outside the scope of this paper.

At the end points of the snare, boundary conditions must be carefully analysed. Let $g_0 = \delta^{(2)}(\mathbf{x} - \boldsymbol{\pi}(0))$ be the distribution function from the end of the snare at $\chi = 0$ to the corresponding point on the membrane $\mathcal{M}_c$. When the snare is attached to the membrane, their displacements must be the same at the end point:

$$u|_{\chi=0} = \int_{\mathcal{M}_c} g_0 \, w_c \, dx \, dy. \tag{17}$$

Furthermore, the force density acting on $\mathcal{M}_c$ at the same point can be written as:

$$\mathcal{F}_0 = g_0 \, f_0, \qquad f_0 = T_s \partial_\chi u|_{\chi=0} + 2\rho_s \sigma_{1,s} \partial_{t\chi} u|_{\chi=0}. \tag{18}$$

These expressions can be easily arrived at through energy analysis techniques (see Sec. 2.6). Analogous conditions can be written for the edge at $\chi = L$.

2.6. Energy balance

A thorough analysis of the model presented above by means of frequency methods can be ruled out, given the simultaneous presence of several interacting components with strongly non-linear couplings and irregular geometry. To this end, an alternative approach is given by energy methods.

One way of calculating the energy of the system is to multiply Eqs. (2), (3), (5), (9) and (12) by the first time derivative of the variable on the left side of the equation, and then to integrate over the corresponding domain (e.g., multiply (2) by $\partial_t w_b$ and integrate over $\mathcal{M}_b$, etc.) Using integration by parts leads to an energy balance and to the determination of suitable boundary and coupling conditions, as outlined below.

An energy balance for the whole system can be arrived at by summing the contributions for the various components, and can be written as

$$\frac{d\mathfrak{H}}{dt} = -\mathfrak{Q} + \mathfrak{B}, \tag{19}$$

where $\mathfrak{H} = \mathfrak{H}_b + \mathfrak{H}_c + \mathfrak{H}_M + \mathfrak{H}_s + \mathfrak{H}_a$ is the total energy of the system, $\mathfrak{Q}$ represents all the loss terms and $\mathfrak{B}$ groups together boundary terms. The explicit expressions for the various contributions to $\mathfrak{H}$ are given below:

$$\mathfrak{H}_i = \int_{\mathcal{M}_i} \frac{\rho_i}{2}(\partial_t w_i)^2 + \frac{T_i}{2}|\nabla_{2D} w_b|^2 \, dx\, dy, \quad i = b, c, \tag{20a}$$

$$\mathfrak{H}_a = \int_{\mathcal{V}} \frac{\rho_a}{2c_a^2}(\partial_t \Psi)^2 + \frac{\rho_a}{2}|\nabla_{3D}\Psi|^2 \, dx\, dy\, dz, \tag{20b}$$

$$\mathfrak{H}_M = \frac{M}{2}\dot{z}_M^2 + \Phi_M, \tag{20c}$$

$$\mathfrak{H}_s = \int_{\mathcal{D}_s} \frac{\rho_s}{2}(\partial_t u)^2 + \frac{T_s}{2}(\partial_\chi u)^2 + \Phi_s \, d\chi, \tag{20d}$$

where ∇_{2D} represents the 2D gradient. In order for the scheme to be energy conserving, all the terms in $\mathfrak{B}$ must sum to zero, and it is indeed the case here, while contributions to $\mathfrak{Q}$ come from the loss terms in the membranes' and snare's equations, plus from absorbing conditions over the boundaries of $\mathcal{V}$. It can be shown that each of these individual terms is positive, thus leading to a net dissipation of energy in the system.

3. FINITE DIFFERENCE SCHEMES

In this section, the implementation of the model described above will be carried out using the finite difference method [18].

The discretisation in space of the various components will be performed over different Cartesian grids in 1D, 2D or 3D depending on the dimension of the domain. Time discretisation, instead, will be unique for the entire system, with temporal step $k = 1/F_s$ defined as the inverse of the sampling frequency F_s. Spatial grid steps can be derived in terms of k according to stability conditions analysed below. A one dimensional function, like $u(\chi, t)$ for example, will be approximated by a discrete function u_l^n, over a grid with step h_s (where n and l represent the time and spatial index, respectively.) However, it is very convenient to represent grid functions as column vectors, regardless of their dimensions. If in the 1D case it is obvious how to perform such operation, in the 2D and 3D cases several options are available. On a 2D grid, points will be grouped columnwise along the y axis, while in the 3D the same operation will be applied to successive horizontal slices along the vertical axis for increasing values of z.

Let $\mathbf{u}^n$ be the vectorised form of u_l^n. For such a variable, one can define forward and backward time shift operators as following:

$$e_{t+}\mathbf{u}^n = \mathbf{u}^{n+1}, \qquad e_{t-}\mathbf{u}^n = \mathbf{u}^{n-1}. \tag{21}$$

Time difference and averaging operators can be obtained from combinations of the previous ones, and are listed in Table 2. Space difference operators, when operating on vectors, can be expressed as matrices [18].

Table 2: *List of time difference and averaging operators.*

Time difference operators	
$\delta_{t+} = (e_{t+} - 1)/k$	forward difference
$\delta_{t-} = (1 - e_{t-})/k$	backward difference
$\delta_{t\cdot} = (e_{t+} - e_{t-})/2k$	centred difference
$\delta_{tt} = (e_{t+} - 2 + e_{t-})/k^2$	second difference
Time averaging operators	
$\mu_{t+} = (e_{t+} + 1)/2$	forward average
$\mu_{t-} = (1 + e_{t-})/2$	backward average
$\mu_{t\cdot} = (e_{t+} + e_{t-})/2$	centred average

3.1. Membranes

Let $\mathbf{w}_i^n$ be the discrete approximations in vector form of the membranes' displacements $w_i(x, y, t)$ over grids of spacing h_i, with $i = b, c$. Equations (2) and (3) can be thus discretised as

$$\rho_b \delta_{tt}\mathbf{w}_b^n = \mathfrak{l}_b[\mathbf{w}_b^n] + \mathfrak{f}_b^{+,n} + \mathfrak{f}_b^{-,n} + \mathfrak{f}_M^n, \tag{22}$$

$$\rho_c \delta_{tt}\mathbf{w}_c^n = \mathfrak{l}_c[\mathbf{w}_c^n] + \mathfrak{f}_c^{+,n} + \mathfrak{f}_c^{-,n} + \mathfrak{f}_s^n + \mathfrak{f}_0^n + \mathfrak{f}_L^n. \tag{23}$$

The operator $\mathfrak{l}_i[\mathbf{w}_i^n]$ is the discrete counterpart of (4):

$$\mathfrak{l}_i[\mathbf{w}_i^n] = T_i \mathbf{D}_{\boxplus,i}\mathbf{w}_i^n - 2\rho_i\sigma_{0,i}\delta_{t\cdot}\mathbf{w}_i^n + 2\rho_i\sigma_{1,i}\delta_{t-}\mathbf{D}_{\boxplus,i}\mathbf{w}_i^n \tag{24}$$

where $\mathbf{D}_{\boxplus,i}$ is the matrix form of the 2D Laplacian Δ_{2D}, which is generally different between the two membrane grids.

3.2. Air

Let $\mathbf{\Psi}^n$ be a discrete approximation of $\Psi(x, y, z, t)$ over a 3D grid of spacing h_a. A finite difference approximation for (5) can be written as

$$\delta_{tt}\mathbf{\Psi}^n = c_a^2 \mathbf{D}_{\boxplus}\mathbf{\Psi}^n + c_a\sigma_a\delta_{t-}\mathbf{D}_{\boxplus}\mathbf{\Psi}^n, \tag{25}$$

where $\mathbf{D}_{\boxplus}$ is the matrix representation of the 3D Laplacian Δ_{3D}.

The last term introduces a frequency-dependent loss that increases with frequency. It is critical to include viscothermal losses in this model in order to suppress spurious artefacts that are perceptually very relevant. More will be said about this in Sec. 5.3.

The implementation of boundary conditions over the shell, absorbing conditions over the walls and coupling conditions with the membranes will be omitted, as they have been analysed several times in recent works. The interested reader is referred to [4, 5].

3.3. Mallet

Let z_M^n and f_b^n be the sampled versions at time $t = nk$ of $z_M(t)$ and $f_b(t)$, respectively. Equation (9) becomes:

$$M\delta_{tt} z_M^n = f_b^n, \qquad \mathfrak{f}_b^n = -\mathbf{g}_b f_b^n, \tag{26}$$

where $\mathbf{g}_b$ is a column vector representing the distribution $g_b(x, y)$. Normalisation is obtained by imposing $h_b^2 \mathbf{1}^T \mathbf{g}_b = 1$, where $\mathbf{1}^T$ is the transpose of a column vector consisting of ones.

As discussed in Sec. 2.4, f_b^n can be expressed in terms of a discrete potential Φ_M^n:

$$f_b^n = \frac{\delta_{t\cdot}\Phi_M^n}{\delta_{t\cdot}\eta^n}, \qquad \eta^n = h_b^2 \mathbf{g}_b^T \mathbf{w}_b^n - z_M^n, \tag{27}$$

where $\Phi_M^n = \Phi_M(\eta^n)$.

3.4. Snare

The displacement $u(\chi, t)$ of the snare can be represented by the vector $\mathbf{u}^n$, over a 1D grid of spacing h_s. Equation (12) can be written as:

$$\rho_s \delta_{tt} \mathbf{u}^n = T_s \mathbf{D}_{\chi\chi} \mathbf{u}^n - 2\rho_s \sigma_{0,s} \delta_{t\cdot} \mathbf{u}^n + \\ + 2\rho_s \sigma_{1,s} \delta_{t-} \mathbf{D}_{\chi\chi} \mathbf{u}^n - \mathfrak{f}_e^n, \tag{28}$$

where $\mathbf{D}_{\chi\chi}$ is the matrix representation of the operator $\partial_{\chi\chi}$. The discrete version $\mathfrak{f}_s$ of the collision force density $\mathcal{F}_s$ in (14) is defined as:

$$\mathfrak{f}_s^n = \mathbf{G}_s \mathfrak{f}_e^n, \tag{29}$$

where $\mathbf{G}_s$ is the matrix form of the linear operator $\int_{\mathcal{D}_s} G_s(\,\cdot\,)\, d\chi$. As in the mallet case, it is possible to express $\mathfrak{f}_e$ in terms of a discrete potential $\mathbf{\Phi}_s^n$

$$\mathfrak{f}_e^n = \frac{\delta_{t\cdot}\mathbf{\Phi}_s^n}{\delta_{t\cdot}\boldsymbol{\xi}^n}, \tag{30}$$

$$\mathbf{\Phi}_s^n = \frac{\kappa_s}{\beta+1} [\boldsymbol{\xi}^n]_+^{\beta+1}, \qquad \boldsymbol{\xi}^n = \mathbf{u}^n - \mathbf{G}_s^T \mathbf{w}_c^n. \tag{31}$$

The vector by vector division in (30) is intended here and in the remainder of the article as an element-by-element operation.

At the end point $l = 0$, continuous boundary conditions (17) and (18) can be discretised as

$$u_0^n = h_c^2 \mathbf{g}_0^T \mathbf{w}_c^n, \tag{32a}$$

$$\mathfrak{f}_0^n = \mathbf{g}_0 f_0^n, \quad f_0^n = (T_s \delta_{\chi-} + 2\rho_s \sigma_{1,s} \delta_{t-} \delta_{\chi-}) u_0^n, \tag{32b}$$

where $\mathbf{g}_0$ is the discrete approximation of the distribution g_0. Analogous expressions can be found for the other end point. When applied to the grid point u_0^n, the operator $\delta_{\chi-}$ would give:

$$\delta_{\chi-} u_0^n = (u_0^n - u_{-1}^{*,n})/h_s. \tag{33}$$

As $u_{-1}^{*,n}$ lies outside of the 1D grid, it is sometimes called virtual or ghost point (hence the notation *). Equation (32b) must be considered as a formal way of determining suitable update conditions for the scheme (see Sec. 4.2.)

3.5. Energy and Stability

In the numerical case, an energy balance corresponding to (19) can be written as:

$$\delta_{t-} \mathfrak{h}^{n+1/2} = -\mathfrak{q}^n + \mathfrak{b}^n, \tag{34}$$

where $\mathfrak{h}^{n+1/2}$ is the numerical energy of the system at time $(n+1/2)k$, $\mathfrak{q}^n$ represents losses and $\mathfrak{b}^n$ the boundary terms. As in the continuous case, $\mathfrak{h}^{n+1/2}$ can be written as a sum of the following terms:

$$\mathfrak{h}_i^{n+1/2} = h_i^2 \left(\frac{\rho_i}{2} |\delta_{t+} \mathbf{w}_i^n|^2 + \frac{T_i}{2} ((\mathbf{D}_{x+} \mathbf{w}_i^n)^T \cdot e_{t+}(\mathbf{D}_{x+} \mathbf{w}_i^n)) \right. \\ \left. + \frac{T_i}{2} ((\mathbf{D}_{y+} \mathbf{w}_i^n)^T \cdot e_{t+}(\mathbf{D}_{y+} \mathbf{w}_i^n)) \right), \quad i = b, c, \tag{35}$$

$$\mathfrak{h}_a^{n+1/2} = h_a^3 \left(\frac{\rho_a}{2c_a^2} |\delta_{t+} \mathbf{\Psi}^n|^2 + \frac{\rho_a}{2} ((\mathbf{D}_{x+} \mathbf{\Psi}^n)^T \cdot e_{t+}(\mathbf{D}_{x+} \mathbf{\Psi}^n)) \right. \\ + \frac{\rho_a}{2} ((\mathbf{D}_{y+} \mathbf{\Psi}^n)^T \cdot e_{t+}(\mathbf{D}_{y+} \mathbf{\Psi}^n)) \\ \left. + \frac{\rho_a}{2} ((\mathbf{D}_{z+} \mathbf{\Psi}^n)^T \cdot e_{t+}(\mathbf{D}_{z+} \mathbf{\Psi}^n)) \right), \tag{36}$$

$$\mathfrak{h}_M^{n+1/2} = \frac{M}{2} (\delta_{t+} z_M^n)^2 + \mu_{t+} \Phi_M^n, \tag{37}$$

$$\mathfrak{h}_s^{n+1/2} = h_s \left(\frac{\rho_s}{2} |\delta_{t+} \mathbf{u}^n|^2 + \frac{T_s}{2} ((\mathbf{D}_{\chi+} \mathbf{u}^n)^T \cdot e_{t+}(\mathbf{D}_{\chi+} \mathbf{u}^n)) \right. \\ \left. + \mathbf{1}^T \mu_{t+} \mathbf{\Phi}_s^n \right), \tag{38}$$

where $|\cdot|$ denotes the Euclidean norm of a vector, and the various difference matrices represent forward spatial difference operators [19]. It is understood that, in the air term, the z derivative be calculated everywhere but across the two membranes. The boundary term $\mathfrak{b}^n$ is identically zero. When the system is lossless, and reflective conditions are applied over the walls of the box, the total energy $\mathfrak{h}^{n+1/2}$ is conserved to machine accuracy. See Sec. 5.1 for details. Otherwise, energy is monotonically dissipated.

By requiring that all the energy terms be positive, stability conditions for the schemes can be arrived at. For the membranes and snare schemes, the presence of collisions does not alter the usual conditions:

$$h_i^2 \geq 2k^2 T_i/\rho_i + 8\sigma_{1,i} k, \quad i = b, c, \tag{39}$$

$$h_s^2 \geq k^2 T_s/\rho_s + 4\sigma_{1,s} k. \tag{40}$$

For the air scheme, stability condition depends on σ_a:

$$h_a^2 \geq 3c_a^2 k^2 + 6c_a \sigma_a k. \tag{41}$$

4. NUMERICAL IMPLEMENTATION

In this section, the numerical implementation of mallet-membrane and snare-membrane collisions will be discussed. In both cases, it is necessary to solve a nonlinear equation at every time step. Existence and uniqueness of solution will be analysed.

4.1. Mallet-membrane collision

Consider the mallet and batter membrane schemes first. The update for the membrane points included in the distribution $\mathbf{g}_b$ will be coupled to the mallet's position by the collision force f_b^n. When all the terms in (22) and (26) are expanded and air coupling is taken

into account, the update expressions for $\mathbf{w}_b^{n+1}$ and z_M^{n+1} can be schematically written as

$$\mathbf{A}_b \mathbf{w}_b^{n+1} = \boldsymbol{\omega}_b^n[\mathbf{w}_b^n, \mathbf{w}_b^{n-1}, \boldsymbol{\Psi}^n, \boldsymbol{\Psi}^{n-1}] - \frac{k^2}{\rho_b}\mathbf{g}_b f_b^n, \tag{42}$$

$$z_M^{n+1} = \zeta_M^n[z_M^n, z_M^{n-1}] + k^2 f_b^n / M, \tag{43}$$

where $\mathbf{A}_b$ is a symmetric, positive definite matrix due to losses and air coupling, and $\boldsymbol{\omega}_b^n$ and ζ_M^n represent linear combinations of known terms from previous time steps. These two components can be updated by finding η^{n+1} first, then by calculating f_b^n and finally by inserting it in (42) and (43). To this end, start by inverting the system (42) and by multiplying it by $h_b^2 \mathbf{g}_b^T$, then subtract (43). After a brief calculation, it is possible to write a nonlinear equation in $r^n = \eta^{n+1} - \eta^{n-1}$ which must be solved at every time step:

$$r^n + \gamma \frac{\Phi_M(r^n + a^n) - \Phi_M(a^n)}{r^n} + b^n = 0, \tag{44}$$

where

$$\gamma = \frac{h_b^2 \mathbf{g}_b^T \mathbf{A}_b^{-1} \mathbf{g}_b k^2}{\rho_b} + \frac{k^2}{M}, \qquad a^n = \eta^{n-1}, \tag{45a}$$

$$b^n = \zeta^n - h_b^2 \mathbf{g}_b^T \mathbf{A}_b^{-1} \boldsymbol{\omega}_b^n + \eta^{n-1}. \tag{45b}$$

The particular choice of a power law nonlinearity for Φ_M guarantees a unique solution for (44), as has been shown in [13] for a simpler case.

4.2. Snare-membrane collision

The implementation of the snare-membrane interaction is somewhat complicated by the fact that the snare is a distributed object, and by the presence of air coupling and boundary conditions at the end points. As before, Eqs. (23) and (28) can be schematically written as

$$\mathbf{w}_c^{n+1} = \mathbf{A}_c^{-1} \boldsymbol{\omega}_c^n + \frac{k^2}{\rho_c} \mathbf{A}_c^{-1} \left(\mathbf{g}_0 f_0^n + \mathbf{g}_L f_L^n + \mathbf{G}_s \mathfrak{f}_e^n\right) \tag{46}$$

$$\mathbf{u}^{n+1} = \boldsymbol{\upsilon}^n / q_s - k^2 \mathfrak{f}_e^n / (\rho_s q_s), \tag{47}$$

where $\boldsymbol{\omega}_c^n[\mathbf{w}_c^n, \mathbf{w}_c^{n-1}, \boldsymbol{\Psi}^n, \boldsymbol{\Psi}^{n-1}]$ and $\boldsymbol{\upsilon}^n[\mathbf{u}^n, \mathbf{u}^{n-1}]$ depend on known values of the various variables, $\mathbf{A}_c$ is a constant matrix analogous to $\mathbf{A}_b$ and $q_s = 1 + \sigma_{0,s} k$.

One way to proceed in order to solve this system is to start by solving for the pointwise forces f_0 and f_L. Using (32b), it is possible to write

$$u_0^{n+1} = -\frac{k^2}{q_s \rho_s} f_0^n + \frac{1}{q_s} \upsilon_0^n, \tag{48}$$

where the first term on the right hand side replaces derivatives that could not otherwise be calculated, and $f_{s,0}^n = 0$ because the snare and the membrane are attached. By multiplying (46) by $h_c^2 \mathbf{g}_0^T$ and by imposing condition (32a), it is possible to write f_0^n in terms of the (still unknown) force density $\mathfrak{f}_e^n$:

$$f_0^n = \phi_0^n - \boldsymbol{\nu}^T \mathfrak{f}_e^n, \tag{49}$$

with ϕ_0^n combination of known terms and $\boldsymbol{\nu}$ a constant vector. A similar process can be repeated for f_L.

Now, after substituting these expressions for f_0^n and f_L^n back into (46), it is possible to follow the same procedure used for the mallet-membrane case. Multiplying (46) by $h_c^2 \mathbf{G}_s^T$ and subtracting this from (47) leads to a nonlinear equation in the unknown vector $\mathbf{r}^n = \boldsymbol{\xi}^{n+1} - \boldsymbol{\xi}^{n-1}$ formally similar to (44):

$$\mathbf{r}^n + \boldsymbol{\Gamma} \frac{\boldsymbol{\Phi}_s(\mathbf{r}^n + \mathbf{a}^n) - \boldsymbol{\Phi}_s(\mathbf{a}^n)}{\mathbf{r}^n} + \mathbf{b}^n = 0, \tag{50}$$

where $\boldsymbol{\Gamma}$ is a constant, symmetric and positive definite matrix, and $\mathbf{b}^n$ and $\mathbf{a}^n$ depend only on known values. Once this equation is solved, it is possible to calculate $\mathfrak{f}_e^n$, and therefore to update the rest of the scheme explicitly. Uniqueness of a solution in the vector case is guaranteed by the special form of $\boldsymbol{\Gamma}$ [20].

As explained in Sec. 2, the present analysis has concentrated on a single snare for simplicity sake. However, it is straightforward to extend the derivation of the previous section to $N_s > 1$ snares. The grid values for the various snares can be consolidated in a single vector, and expressions like (50) still hold. Conditions involving the end points, instead, will be transformed into vectors of size N_s, and their values will generally be coupled.

5. RESULTS

5.1. Energy conservation

As discussed in Sec. 3.5, the numerical energy of the system can be calculated, and must remain constant to machine accuracy in the lossless case and without absorbing conditions over the walls of $\mathcal{V}$. Figure 2 shows the normalised variations of $\mathfrak{h}$, together with the partition into the various components. Such an energy measure can be extremely useful for debugging purposes, as virtually any error has an impact on the conservation of $\mathfrak{h}$. The drum is excited by a mallet with $M = 0.028$ kg and initial velocity $v = -5$ m/s at $t = 0$ s. Seven snares are included in the model.

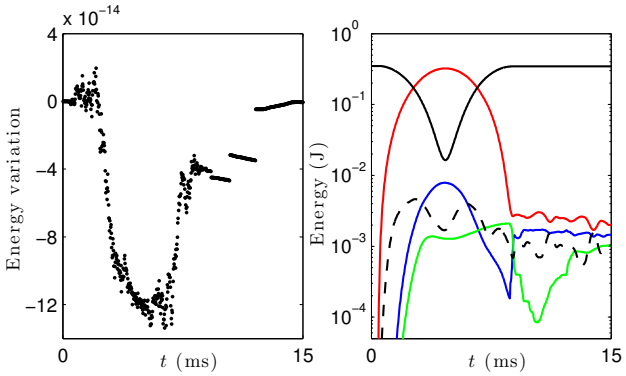

Figure 2: Left: normalised variations of the total energy $\mathfrak{h}$ for a snare drum in the lossless case. Right: contribution to the total energy given by the various components (solid black: mallet, red: upper membrane, blue: lower membrane, dashed black: air, green: snares). The sample rate is 44 100 Hz.

5.2. Evolution of the system

Figure 3 schematically illustrates what happens when the drum is excited with parameters given in the previous section. A positive pressure due to the compression of the membrane is generated inside the cavity, which pushes the lower membrane downwards,

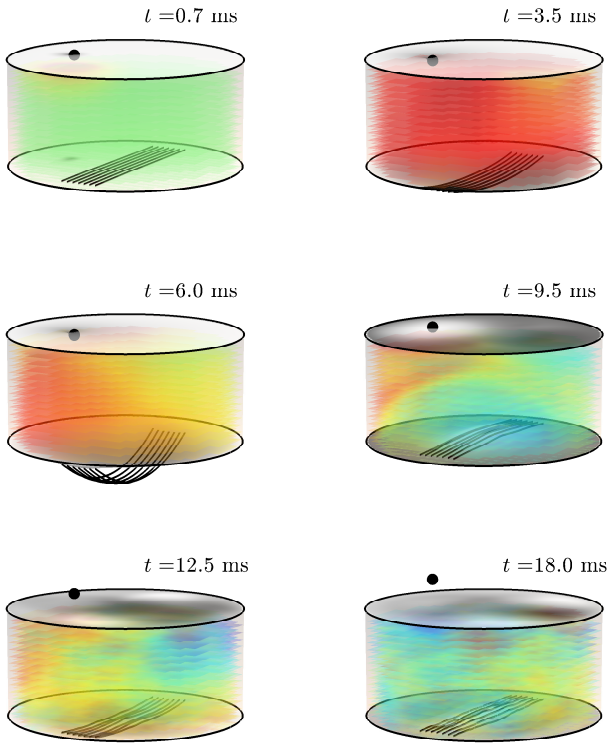

Figure 3: Snapshots of the evolution of the snare drum system at times as indicated. The pressure variations from atmospheric inside the cavity are depicted (green: zero variation, red: positive variation, blue: negative variation.) Displacements have been altered for illustration purposes.

together with the snares. The snares reach their maximum displacement at $t = 6$ ms, when they start to move upwards. At about $t = 9$ ms, the snares hit the membrane almost coherently (notice the pressure wave generated by the impact). At later times, the behaviour of the snares becomes rapidly chaotic.

5.3. A note on dispersion error, ABCs and viscosity

It is well-known for the lossless case ($\sigma_a = 0$ m) that the scheme employed for the 3D air box exhibits significant dispersion error [21]. Dispersion error essentially means that the ideal linear relationship between temporal and spatial frequencies is warped in the finite difference scheme. Numerical wave speed is thus dependent on direction and frequency. In this case, high frequencies tend to lag along the axial directions. While more accurate schemes exist for minimising dispersion, such as interpolated schemes [21], due to the complexity of the full 3D drum embedding presented here and with the goal of presenting a complete energy analysis, such schemes are currently distant options. This 3D scheme is often used with a large oversampling of the grid in order to reduce dispersion error to acceptable levels, such as in [3] where a 24 kHz sampling rate was used for a 700 Hz output. The full audible bandwidth is of interest here so oversampling was not employed, since computational costs rise drastically when reducing the time-step (16x increase for doubling of the sampling rate).

The presence of dispersion error causes some challenges when absorbing boundary conditions (ABCs) are used. The absorbing boundaries employed here are of the first-order Engquist-Majda type:

$$(\partial_t - c_a \mathbf{n} \cdot \vec{\nabla}_{3D})\Psi = 0\,, \quad (x, y) \in \partial\mathcal{V}. \tag{51}$$

The problem that is encountered with this condition (and any ABC for that matter), is that it assumes the wave speed to be constant, but in the finite difference scheme the numerical wave speed is directionally and frequency-dependent [21]. Another problem with condition (51) is that it is less effective for incoming waves that are not normal to the boundary. Ultimately, these two effects combine such that the ABCs only partially absorb incident waves. This can be seen in the spectrogram displayed in Fig. 4a, which refers to the output of a simulation without viscosity in the air ($\sigma_a = 0$ m) and without the cavity or snares. The output was taken along a diagonal above the top membrane and the spectrogram uses a 512 sample Hann window with 75% overlap. It can be seen there is energy which is slow to decay at approximately 8643 Hz. This is in fact the temporal frequency ($0.196F_s$) that experiences the worst dispersion error (approx. 30% error) for axial-directed waves [21]. There is another peak at $0.304F_s$, which is the temporal frequency pertaining to the worst error for side-diagonal directions (approx. 25% error) [21].

When the cavity and snares are added to the simulation there is an increase in mid-frequency energy due to the modes of the cavity and due to the snares activity. A spectrogram for this case is shown in Fig. 4b. In this case, the energy that is slow to decay causes audible 'hiss' and 'ringing' artefacts. Although not presented here, higher-order ABCs (up to fourth order) were also not effective at reducing this effect. Fortunately, viscosity in air has a damping effect that targets high frequencies [14]. A spectrogram from the same listening position, now with $\sigma_a = 2 \times 10^{-6}$ m, is shown in Fig. 4c. It can be seen that the energy in this band of frequencies decays faster than in the lossless case. It was found that this added decay was sufficient to eliminate the audible artefacts.

5.4. Sounds and Videos

Sound examples and videos can be found at the author's website:
`www2.ph.ed.ac.uk/~s1164558`

6. FINAL REMARKS

In this paper, a physics-based model of a snare drum has been presented. A novel, energy conserving numerical scheme for the simulation of collisions has been discussed, which can be applied both to the mallet-membrane and to the snare-membrane interactions. This constitutes a major improvement with respect to previous works, as in this case the stability of the numerical scheme can be guaranteed.

Another problem that has been discussed in this work is the effect of dispersion in the 3D Cartesian scheme in virtual embedding simulations such as this. It has been found that, when high frequencies are created in the model, either by the mallet or by the snares, a slowly attenuating "hiss" is produced, which dominates the spectrogram of the output sound and harms its quality. This problem has been interpreted as dispersion of the 3D scheme exacerbating the proper functioning of absorbing boundary conditions. However, when viscothermal effects are added to the 3D scheme these artefacts are rendered inaudible.

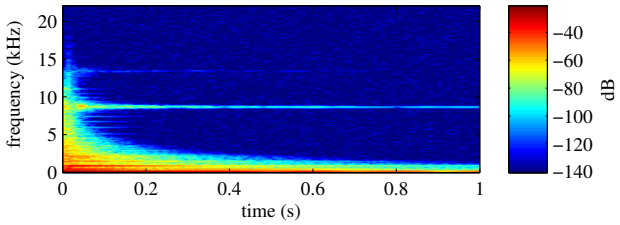

(a) *Without cavity, snares and viscosity*

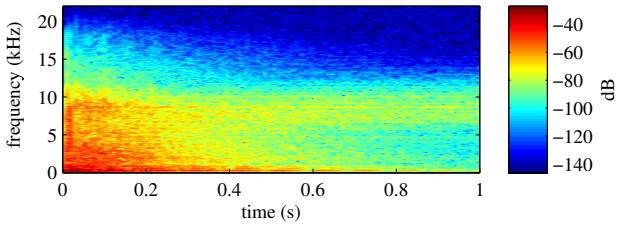

(b) *With cavity and snares, without viscosity*

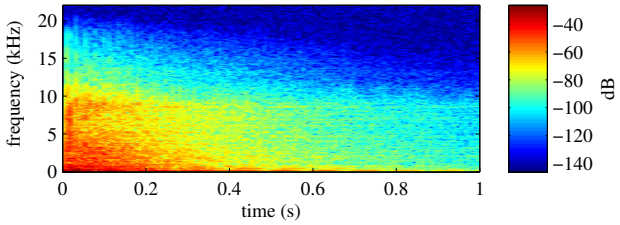

(c) *With cavity, snares and viscosity*

Figure 4: *Spectrograms for simulation output.*

A point which has not been mentioned in this work is the computation cost of this model. As discussed in Sec. 4, the collision model presented relies on the solution of a nonlinear equation with the Newton-Raphson method at every time step. If in the case of the mallet this is just a scalar equation, it becomes a challenging problem for the snares-membrane interaction, where a vectorial equation is involved. When a realistic number of snares is included in the numerical model, the dominant part of the code in terms of computation time is the solution of the nonlinear system (50), and not, as one would expect, the update of the 3D field. The former, in fact, requires the iterative solution of a linear system, which in this case is dense. It is, therefore, an intrinsic serial operation. As well known, parallel hardware like GPGPUs can be extremely useful in accelerating the computation of systems with a high degree of parallelisability, and this is becoming a mainstream approach to room acoustics simulation [22]. However, this hardware is not suited for cases like the present one, where operations must be performed in a sequential order. One of the major challenges at the moment is to find alternative methods that could tackle more effectively this problem.

7. REFERENCES

[1] J. A. Laird, *The physical modelling of drums using digital waveguides*, Ph.D. thesis, University of Bristol, 2001.

[2] F. Avanzini and R. Marogna, "A modular physically based approach to the sound synthesis of membrane percussion instruments," *Audio, Speech, and Language Processing, IEEE Transactions on*, vol. 18, no. 4, pp. 891–902, 2010.

[3] L. Rhaouti, A. Chaigne, and P. Joly, "Time-domain modeling and numerical simulation of a kettledrum," *The Journal of the Acoustical Society of America*, vol. 105, pp. 3545, 1999.

[4] S. Bilbao, "Time domain simulation and sound synthesis for the snare drum," *The Journal of the Acoustical Society of America*, vol. 131, pp. 914–925, 2012.

[5] A. Torin and S. Bilbao, "Numerical experiments with non-linear double membrane drums," in *Proc. 4th Stockholm Musical Acoustics Conference (SMAC 2013)*, Stockholm, Sweden, 2013.

[6] P. Wriggers, *Computational Contact Mechanics*, Springer-Verlag Berlin Heidelberg, second edition, 2006.

[7] F. Avanzini and D. Rocchesso, "Modeling collision sounds: Non-linear contact force," in *Proc. COST-G6 Conf. Digital Audio Effects (DAFx-01)*, Limerick, Ireland, 2001, pp. 61–66.

[8] A. Chaigne and A. Askenfelt, "Numerical simulations of piano strings. I. A physical model for a struck string using finite difference methods," *The Journal of the Acoustical Society of America*, vol. 95, no. 2, pp. 1112–1118, 1994.

[9] J. Chabassier, *Modélisation et simulation numérique d'un piano par modèles physiques.*, Ph.D. thesis, Ecole Polytechnique X, 2012.

[10] D. Kartofelev, A. Stulov, H.-M. Lehtonen, and V. Välimäki, "Modeling a vibrating string terminated against a bridge with arbitrary geometry," in *Proc. 4th Stockholm Musical Acoustics Conference (SMAC13)*, Stockholm, Sweden, 2013.

[11] D. Greenspan, "Conservative numerical methods for $\ddot{x} = f(x)$," *Journal of Computational Physics*, vol. 56, no. 1, pp. 28–41, 1984.

[12] S. Li and L. Vu-Quoc, "Finite difference calculus invariant structure of a class of algorithms for the nonlinear klein-gordon equation," *SIAM Journal on Numerical Analysis*, vol. 32, no. 6, pp. 1839–1875, 1995.

[13] V. Chatziioannou and M. van Walstijn, "An energy conserving finite difference scheme for simulation of collisions," in *Proc. of the Sound and Music Computing Conference (SMC 2013)*, Stockholm, Sweden, 2013, pp. 584–591.

[14] P. M. Morse and K. U. Ingard, *Theoretical acoustics*, McGraw-Hill Inc., USA, 1986.

[15] B. Engquist and A. Majda, "Absorbing boundary conditions for numerical simulation of waves," *Proceedings of the National Academy of Sciences*, vol. 74, no. 5, pp. 1765–1766, 1977.

[16] J. G. Meloney and K. E. Cummings, "Adaptation of FDTD techniques to acoustic modeling," in *11th Annual Review of Progress in Applied Computational Electromagnetics*, 1995, vol. 2, pp. 724–731.

[17] K. Hunt and F. Crossley, "Coefficient of restitution interpreted as damping in vibroimpact," *Journal of applied mechanics*, vol. 42, no. 2, pp. 440–445, 1975.

[18] B. Gustafsson, H.-O. Kreiss, and J. Oliger, *Time dependent problems and difference methods*, Wiley New York, 1995.

[19] S. Bilbao, *Numerical Sound Synthesis: Finite Difference Schemes and Simulation in Musical Acoustics*, Wiley Publishing, Chichester, UK, 2009.

[20] S. Bilbao, A. Torin, and V. Chatziioannou, "Numerical modeling of collisions in musical instruments," *Under review*, vol. available online at http://arxiv.org/abs/1405.2589, 2014.

[21] K. Kowalczyk and M. van Walstijn, "Room acoustics simulation using 3-D compact explicit FDTD schemes," *Audio, Speech, and Language Processing, IEEE Transactions on*, vol. 19, no. 1, pp. 34–46, 2011.

[22] C. J. Webb and S. Bilbao, "Computing room acoustics with CUDA-3D FDTD schemes with boundary losses and viscosity," in *Acoustics, Speech and Signal Processing, IEEE International Conference on*, Prague, Czech Republic, 2011, IEEE, pp. 317–320.